

Heat rectification by two qubits coupled with Dzyaloshinskii–Moriya interaction

Vipul Upadhyay,¹ M. Tahir Naseem,² Rahul Marathe,^{1,*} and Özgür E. Müstecaplıoğlu^{2,†}

¹*Department of Physics, Indian Institute of Technology Delhi, Hauz Khas 110 016, INDIA*

²*Department of Physics, Koç University, 34450 Sariyer, Istanbul, Turkey*

We investigate heat rectification in a two-qubit system coupled via the Dzyaloshinskii–Moriya (DM) interaction. We derive analytical expressions for heat currents and thermal rectification and provide possible physical mechanisms behind the observed results. We show that the anisotropy of DM interaction in itself is not sufficient for heat rectification to occur, and some other form of asymmetry is needed. We employ off-resonant qubits as the source of this asymmetry. We find the regime of parameters for higher rectification factors by examining the analytical expressions of rectification obtained from a global master equation solution. In addition, it is shown that the direction and quality of rectification can be controlled via various system parameters. Furthermore, we compare the influence of different orientations of the DM field anisotropy on the performance of heat rectification.

I. INTRODUCTION

Manipulation of heat at the nanoscale, particularly thermal rectification by heat diodes, is currently a subject of intense theoretical [1–13] and experimental [14–19] research. The theoretical studies explain the change of heat current direction and magnitude when the thermal bias is reversed due to inherent asymmetry and non-linearity in the physical models [20, 21]. The most common naturally occurring interaction used in such quantum models is the Heisenberg exchange interaction [1–3] where the asymmetry stems from either the different on-site magnetic fields [3] or from the different coupling constants of the subsystem with their respective baths [4].

Recently, an artificially designed system containing inherent asymmetry in the Hamiltonian itself has also been proposed to operate under symmetric system-bath couplings and resonant (identical) subsystems, which allows for the rectification of large heat currents [5]. The model is based upon coupling z -component of a spin to x -component of the other spin in a two qubit system. The coupling is, therefore, asymmetric under the exchange of the spins. This artificial model takes only one of the two terms of the y component of the two spins' cross product. Intriguingly, there is a naturally existing, entirely physical interaction depending on the cross product of the spins, known as Dzyaloshinskii Moriya (DM) interaction [22, 23]. It is antisymmetric under the exchange of spins due to its cross-product dependence. Accordingly, we ask whether DM interaction's anti-symmetry is sufficient per se to generate heat rectification and, even if it is not, how it influences the heat conduction properties. To answer this question, we take a simple system of two DM coupled spin-1/2 particles (qubits) with the DM field along z direction and analytically derive the quantum master equation and heat current expression for our model. We also derive an analytical expression for the rectification factor and discuss the behavior of our model under various parameter limits, providing possible physical mechanisms for the same. We provide the

possible configuration for optimizing the working of our *heat rectifier*. Finally, we explore the role of change of anisotropy field direction on the heat current and rectification ability.

Some effects of DM interaction on heat transport in spin chains have been studied [24, 25]. In particular, possible control of heat rectification using DM interaction in a system of two quantum dots has been proposed [26]. Another study of magnetic thermal rectification in a single molecule magnet concluded that thermal rectification is possible due to anti-symmetry of DM interaction [27]. On the other hand, these studies include the exchange interaction next to the DM interaction, as such an interaction is naturally occurring. However, this may not reveal the role of the DM interaction on heat current per se. Here, we present a more systematic analysis by focusing on the DM interaction alone and investigate symmetry in heat flow in various parameter regimes. In addition, our analysis based on the derivation of a global master equation [28, 29] and analytical results for both heat currents and rectification reveals the underlying mechanism that leads to thermal rectification. Based on the analytical results of rectification, we find the parameters regime for higher rectification factors, thereby guiding further development of thermal devices based on DM interaction. We believe, such systematic analysis has not been done in previous studies of DM interaction-based heat rectifiers. Such a methodological examination of the DM interaction can also be experimentally feasible [18].

Rest of the paper is organized as follows. In Sec. II, we introduce our model and physical system. Section III gives the derivation of the master equation describing the open system dynamics of the model. In Sec. IV, we discuss the analytical solution of the master equation in a series of subsections. First, Sec. IV A presents the heat currents, followed by the rectification abilities of the model system in Sec. IV B. Sec. IV C compares the models with anisotropy fields in different directions. We conclude in Sec. V. Additional details of the derivation of the master equation and the heat currents are provided in Appendices A and B, respectively.

* maratherahul@physics.iitd.ac.in

† omustecap@ku.edu.tr

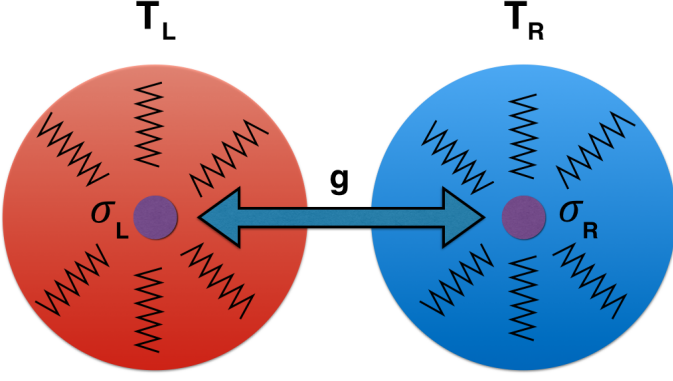


FIG. 1. (Color online) A schematic of the model consisting of two qubits coupled by the Dzyaloshinskii-Moriya (DM) interaction with on-site (local) magnetic fields. Each qubit is attached to its own local bath.

II. THE MODEL

Our physical system consists of two spin-1/2 particles (qubits) coupled via the Dzyaloshinskii-Moriya (DM) interaction in the presence of on-site magnetic fields, which is effectively realizable in nuclear magnetic resonance (NMR) experiments [18]. Each qubit interacts with its own (local) bath at different temperatures, as illustrated in Fig. 1. The Hamiltonian of the system is expressed as

$$H_S = H_0 + H_{DM}, \quad (1)$$

where H_0 is the Hamiltonian of the non-interacting qubits, (we take reduced Planck constant as $\hbar = 1$)

$$\hat{H}_0 = \frac{\omega_L}{2} \hat{\sigma}_L^z \otimes \hat{I}_R + \hat{I}_L \otimes \frac{\omega_R}{2} \hat{\sigma}_R^z, \quad (2)$$

and the DM interaction is described by the Hamiltonian,

$$H_{DM} = g(\hat{\sigma}_L^x \hat{\sigma}_R^y - \hat{\sigma}_L^y \hat{\sigma}_R^x). \quad (3)$$

Here, $\hat{\sigma}_i^\alpha$'s denote the $\alpha = x, y, z$ components of the Pauli spin-1/2 operators for the left ($i = L$) and right ($i = R$) qubits. The unit operators are denoted by \hat{I}_i . We assume on-site magnetic fields can be used for locally distinct frequencies ω_L and ω_R for the left and right qubits, respectively. The DM coupling coefficient g corresponds to the case where the DM anisotropy field is aligned in the z -direction so that the general DM interaction $\mathbf{D} \cdot (\boldsymbol{\sigma}_L \times \boldsymbol{\sigma}_R)$ reduces to Eq. (3) with $\mathbf{D} = g\hat{z}$.

We take the spin-boson model to describe dissipative coupling of each qubit to its respective local bath. Free Hamiltonian of each bath B_i is given by

$$\hat{H}_{B_i} = \sum_n \omega_n \hat{a}_{i,n}^\dagger \hat{a}_{i,n}, \quad (4)$$

where $\hat{a}_{i,n}^\dagger$ ($\hat{a}_{i,n}$) are the bosonic creation (annihilation) operators of the n -th mode of the i th bath. The system-bath interaction is described by

$$\hat{H}_{SB} = \sum_{i,n} g_{i,n} \hat{\sigma}_x^i \otimes (\hat{a}_{i,n}^\dagger + \hat{a}_{i,n}), \quad (5)$$

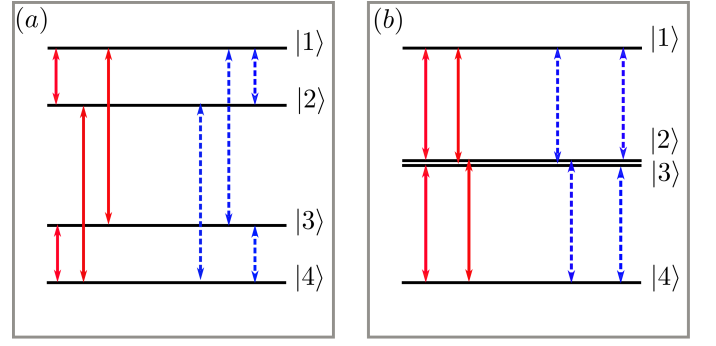


FIG. 2. (Color online) Energy transitions induced by left (solid lines) and right (dashed lines) baths for weakly coupled (a) off-resonant qubits, and (b) for nearly-resonant qubits.

where $g_{i,n}$ represents the coupling coefficient of the n -th mode of the bath B_i to the qubit labeled with i . We assume symmetric couplings between the baths and the qubits such that $g_{L,n} = g_{R,n} \equiv g_n$.

III. MASTER EQUATION

The master equation for our model is derived under the usual Born-Markov and secular approximations, which can be written in the interaction picture as [24]

$$\frac{d}{dt} \hat{\rho}_S(t) = \mathcal{L}_L \hat{\rho}_S(t) + \mathcal{L}_R \hat{\rho}_S(t), \quad (6)$$

where the Liouvillian superoperators are given by

$$\begin{aligned} \mathcal{L}_i \hat{\rho}_S(t) = & \sum_{\omega} \gamma_i(\omega) (\tilde{\sigma}_i^x(\omega) \hat{\rho}_S(t) \tilde{\sigma}_i^{x\dagger}(\omega) \\ & - \frac{1}{2} \{ \tilde{\sigma}_i^{x\dagger}(\omega) \tilde{\sigma}_i(\omega), \hat{\rho}_S(t) \}), \end{aligned} \quad (7)$$

here, $\tilde{\sigma}_i^{x(\dagger)}$ are the jump operators in basis which diagonalize the system Hamiltonian (see Appendix A). Furthermore, γ_i denotes the relaxation rate of the i th bath, and it depends on the form of the heat bath under consideration. In this work, we consider thermal baths with relaxation rates

$$\gamma_i(\omega) = \pi \sum_k |g_i(k)|^2 \delta(\omega_k - \Omega) (1 - e^{-\omega(k)/T_i}). \quad (8)$$

The eigenvalues of the system Hamiltonian (1) are given by

$$\begin{aligned} \pm \omega_S & := \pm \frac{\omega_L + \omega_R}{2}, \\ \pm \Omega & := \pm \sqrt{4g^2 + \omega_D^2}, \end{aligned} \quad (9)$$

where $\omega_D := (\omega_L - \omega_R)/2$ is introduced for brevity of notations. The sign of ω_D tells us which qubit is at higher frequency. The eigenvectors in computational basis associated

with the eigenvalues are expressed as

$$\begin{aligned}
|1\rangle &:= |\omega_S\rangle = |++\rangle, \\
|2\rangle &:= |\Omega\rangle = \cos\theta|+-\rangle + i\sin\theta|-+\rangle, \\
|3\rangle &:= |-\Omega\rangle = i\sin\theta|+-\rangle + \cos\theta|-+\rangle, \\
|4\rangle &:= |-\omega_S\rangle = |--\rangle,
\end{aligned} \tag{10}$$

where the parameter θ is defined as:

$$\cos\theta = \frac{2g}{\sqrt{4g^2 + (\omega_D - \Omega)^2}}, \quad \sin\theta = \frac{\omega_D - \Omega}{\sqrt{4g^2 + (\omega_D - \Omega)^2}}. \tag{11}$$

Energy transitions induced by left and right baths are shown in Fig. 2, which shows that all possible transitions can be induced by both baths. Using the eigenvalues and eigenvectors, the explicit form of the master equation becomes

$$\begin{aligned}
\frac{d\hat{\rho}}{dt} = & \kappa[\cos^2\theta(G_L(\omega_+)\mathcal{D}(\tilde{\sigma}_L^-) + G_L(-\omega_+)\mathcal{D}(\tilde{\sigma}_L^+)) \\
& + \sin^2\theta(G_L(\omega_-)\mathcal{D}(\tilde{\sigma}_L^z\tilde{\sigma}_R^-) + G_L(-\omega_-)\mathcal{D}(\tilde{\sigma}_L^z\tilde{\sigma}_R^+)) \\
& + \cos^2\theta(G_R(\omega_-)\mathcal{D}(\tilde{\sigma}_R^-) + G_R(-\omega_-)\mathcal{D}(\tilde{\sigma}_R^+)) \\
& + \sin^2\theta(G_R(\omega_+)\mathcal{D}(\tilde{\sigma}_L^-\tilde{\sigma}_R^z) + G_R(-\omega_+)\mathcal{D}(\tilde{\sigma}_L^+\tilde{\sigma}_R^z))],
\end{aligned} \tag{12}$$

where $\omega_{\pm} = \omega_S \pm \Omega$, and the dissipator superoperator for a jump operator \hat{A} is defined by,

$$\mathcal{D}(\hat{A}) = \hat{A}\hat{\rho}\hat{A}^\dagger - \frac{1}{2}(\hat{A}^\dagger\hat{A}\hat{\rho} + \hat{\rho}\hat{A}^\dagger\hat{A}). \tag{13}$$

The derivation of Eq. (12) is outlined in Appendix A. For simplicity, we consider flat spectral densities of the baths given by

$$G_i(\omega) = \begin{cases} \kappa_i(1 + N_i(\omega)) & \omega > 0; \\ \kappa_i N_i(|\omega|) & \omega < 0, \end{cases} \tag{14}$$

here, $N_i(\omega)$ is the Bose-Einstein distribution function (we take the Boltzmann constant as $k_B = 1$),

$$N_i(\omega) = \frac{1}{e^{\omega/T_i} - 1}, \tag{15}$$

and κ_i is the coupling strength of a qubit with its own bath, and we assume $\kappa_L = \kappa_R = \kappa$. We have ignored the dephasing term in Eq. (12) because it does not influence the diagonal elements of the density matrix, consequently, it does not affect the steady-state heat currents. We note that, in Eq. (12) non-local jump operators are present, for example, $\tilde{\sigma}_L^z\tilde{\sigma}_R^-$, which means both baths have access to both qubits. Such a master

equation is referred to global master equation which is consistent with the laws of thermodynamics [26, 29]. On contrary, a derivation based on neglecting the interaction term between the qubits leads to a local master equation which may not be consistent with the laws of thermodynamics [27, 29].

IV. RESULTS

For ease in discussion of results we define an asymmetry parameter given as:

$$\epsilon = \frac{|\omega_D|}{2g} \tag{16}$$

which gives us an idea about the relative strength of off resonance in comparison to the DM interaction, we will see later that this quantity allows us to control the diode mechanism. Under this consideration it is easy to show that:

$$\begin{aligned}
\cos^2\theta &= \frac{1}{2\sqrt{1 + \epsilon^2}(\sqrt{1 + \epsilon^2} - \frac{|\omega_D|\epsilon}{\omega_D})}, \\
\sin^2\theta &= \frac{\sqrt{1 + \epsilon^2} - \frac{|\omega_D|\epsilon}{\omega_D}}{2\sqrt{1 + \epsilon^2}}
\end{aligned} \tag{17}$$

From above analysis we can clearly see that for large values of ϵ , depending on the sign of ω_D either $\cos^2\theta$ or $\sin^2\theta$ is very small and other tends to 1, while for small values of ϵ both the function are almost equal and tend to $\frac{1}{2}$.

In this section, we shall make use of the master equation derived in Appendix A to present an analysis of heat flow and heat rectification for various system parameters regimes. We explain rectification results based on different decay rates between the energy levels of the system when the thermal bias is reversed.

A. Heat flow analysis

Heat flux between baths and system is given by [5, 28]

$$I_i = \text{Tr}[\mathcal{L}_i\hat{\rho}_S\tilde{H}_S], \tag{18}$$

where the symbol I_i is used to represent the left I_L or right bath I_R current with the sign convention of positive heat current if the heat flows from the bath to the system and vice versa. According to energy conservation, left and right steady-state heat currents must be equal with opposite signs. Consequently, the evaluation of steady-state right bath current I_R suffices for the qualitative and quantitative analysis of heat flow and thermal rectification. The right bath heat current I_R evaluates to (see Appendix B for details)

$$I_R(T_L, T_R) = \frac{\kappa}{4(1 + \epsilon^2)} \left[\frac{\omega_+(N_R(\omega_+) - N_L(\omega_+))}{D(T_L, T_R, \omega_+)} + \frac{|\omega_-|(N_R(|\omega_-|) - N_L(|\omega_-|))}{D(T_R, T_L, |\omega_-|)} \right], \tag{19}$$

where,

$$D(T_i, T_j, \omega) = \cos^2\theta(2N_i(\omega) + 1) + \sin^2\theta(2N_j(\omega) + 1), \quad (20)$$

and $I_R(T_L, T_R)$ indicates that the left bath temperature T_L is greater than right bath temperature T_R , and it is vice versa for $I_R(T_R, T_L)$. In Eq. (19), heat current I_R depends on the square of DM interaction strength g , accordingly the direction of heat current is independent of anti-symmetric nature of DM interaction. In Fig. 3, heat current I_R is plotted as a function of temperature and coupling strength g . In Fig. 3(a), we verify the analytical result of heat current given in Eq. (19) by comparing it with the result obtained from the numerical solution of Eq. (12). From Fig. 3, it is worth emphasizing on following points: (i) The sign of heat current $I_R(T_L, T_R)$ is independent of the system parameters (ω_S , Ω , and g), it only changes with the interchange of bath temperatures. It is in accordance with the second law of thermodynamics. (ii) For $T_R > T_L$, heat current I_R is positive, which indicates that heat current flows from right to left irrespective of the system parameters, and for $T_L > T_R$ it is vice versa. (iii) For weak coupling g , heat current $I_R(T_L, T_R) < I_R(T_R, T_L)$, which indicates that heat flow is suppressed from left to right, and it can be seen in Fig 3(b). (iv) Higher temperature gradients are associated with larger asymmetric heat flow (Fig. 3(c)). (v) Heat current vanishes for $g = 0; \infty$, accordingly there exists a critical value of g for which heat current is maximum.

To examine the possible physical mechanism behind these observation, we refer to equation (12). There are two channels of heat transfer associated with the decay processes into channels of frequencies ω_{\pm} . For $g = 0$, qubits are uncoupled and there is no heat flow, this can be verified by Eq. (19). As we increase the coupling strength g , the dressed states with energy difference ω_p (Fig. 2) move away from each other so the phonon transfer channel ω_+ becomes of higher energy, as a results of this the current initially increases with increase in g . However, once the energy levels are too far apart for the baths to excite the phonons between them, the current starts decreasing and eventually becomes zero. Taking the high right bath temperature limit of (19), we get, (for $T_R \gg \gg (T_L, \omega_+)$)

$$I_R(T_L, T_R) \approx \frac{\kappa}{4(1 + \epsilon^2)} T_R \left[\frac{1}{\cos^2\theta(2N_L(\omega_+) + 1) + \sin^2\theta(2\frac{T_R}{\omega_+})} + \frac{1}{\sin^2\theta(2N_L(|\omega_-|) + 1) + \cos^2\theta(2\frac{T_R}{|\omega_-|})} \right]. \quad (21)$$

This indicates that $I_R(T_L, T_R)$ linearly increases with T_R and eventually saturates if $\cos^2\theta$, and $\sin^2\theta$ are small. For weakly coupled qubits, either $\cos^2\theta$ or $\sin^2\theta$ is small. Consequently, heat flow saturates for larger temperature gradients. On contrary, heat flow saturates at lower temperature gradients for larger coupling strength g , because both $\cos^2\theta$, and $\sin^2\theta$ have larger values in the strong coupling regime. We note that

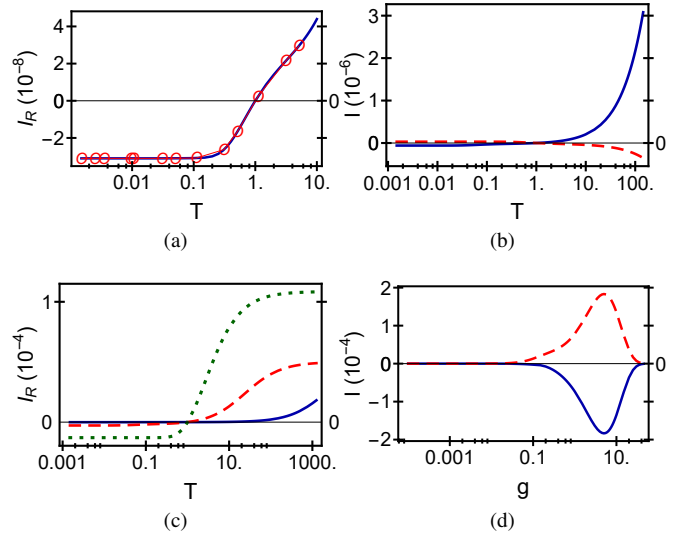


FIG. 3. (Color online) Steady-state right heat bath current I_R as a function of temperature T and coupling strength g . (a) Comparison between the analytical (blue solid line) and numerical (red circles) results of heat current I_R evaluated via Eq. (19) and Eq. (18), respectively. We take $T_{\text{ref}} = 1$ being reference temperature, and $T_R \equiv T, T_L = T_{\text{ref}}$ describes forward-biased configuration. (b) Forward-biased (blue solid line) and reverse-biased (red dashed line) heat current I_R , where reverse-biased (RB) configuration is described by $T_R = T_{\text{ref}}, T_L \equiv T$. (c) Forward-biased (FB) heat current for $g=0.01$ (blue solid line), $g=0.1$ (red dashed line), $g=1$. (green dotted line), and (d) I_R as a function of DM interaction strength g for RB current (blue solid line), and FB current (red dashed line). In both cases, we consider $T_{\text{High}} = 10$, and $T_{\text{Low}} = 1$. Rest of the parameters are given as: $\omega_L = 1$, $\omega_R = 0.1$, $\kappa = 0.0001$, and $g = 0.01$. All the parameters are scaled with the left qubit frequency $\omega_L = 2\pi \times 10$ GHz.

the saturation current is larger for the case with lower ϵ . Interestingly as we will see in Sec. IV B, for better rectification in our model, the heat current saturation should occur at very high temperatures.

B. Heat rectification

Out of the heat current results it is straightforward to calculate the rectification factor which is defined as

$$\mathcal{R} = \frac{I_R(T_R, T_L) + I_R(T_L, T_R)}{\text{Max}[|I_R(T_L, T_R)|, |I_R(T_R, T_L)|]}. \quad (22)$$

We note that, here rectification factor \mathcal{R} is based on the heat current I_R , however, identical results can be obtained replacing I_R with left bath current I_L . The rectification factor \mathcal{R} can take any value between -1 and 1, where $\mathcal{R} = 1, -1$ describes perfect rectification, and $\mathcal{R} = 0$ shows no asymmetry in the heat flow. In addition, $\mathcal{R} > 0$ means heat flow is suppressed from left to right, and $\mathcal{R} < 0$ identifies the opposite case. To explain the physical mechanism behind rectification, we write the rate equation for population dynamics from the

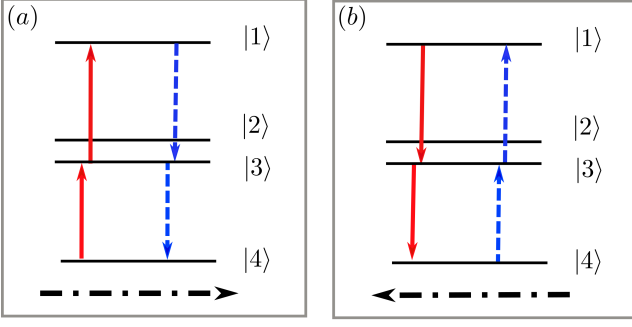


FIG. 4. (Color online) Example of the process that transfers heat between the baths. The dressed states of the weakly interacting resonant qubits $\omega_L = \omega_R = \omega \gg g$. The separation between energy levels $|2\rangle$, and $|3\rangle$ become $4g$, and ω_{\pm} transitions reduce to $\omega \pm 2g$. Solid, and dashed arrows indicate the transitions induced by left and right baths, respectively, and thickness of the arrows reflect decay rate between the states. In addition, dot-dashed arrows point the direction of the heat flow. For resonant qubits, all transition rates become symmetrical under the change in temperature bias due to which rectification becomes zero.

master equation(12)

$$\frac{d}{dt} \begin{bmatrix} \rho_{11} \\ \rho_{22} \\ \rho_{33} \\ \rho_{44} \end{bmatrix} = \begin{pmatrix} -(r3+r4) & r1 & r2 & 0 \\ r3 & -(r1+r4) & 0 & r2 \\ r4 & 0 & -(r2+r3) & r1 \\ 0 & r4 & r3 & -(r1+r2) \end{pmatrix} \begin{bmatrix} \rho_{11} \\ \rho_{22} \\ \rho_{33} \\ \rho_{44} \end{bmatrix} \quad (23)$$

where $r1, r3$ are the transitions rates in ω_- channel and $r2, r4$ are the transitions rates in ω_+ channel given as:

$$\begin{aligned} r1 &= \kappa [\sin^2\theta N_L(|\omega_-|) + \cos^2\theta N_R(|\omega_-|)], \\ r2 &= \kappa [\cos^2\theta N_L(\omega_+) + \sin^2\theta N_R(\omega_+)], \\ r3 &= \kappa [\sin^2\theta e^{\frac{|\omega_-|}{T_L}} N_L(|\omega_-|) + \cos^2\theta e^{\frac{|\omega_-|}{T_R}} N_R(|\omega_-|)], \\ r4 &= \kappa [\cos^2\theta e^{\frac{\omega_+}{T_L}} N_L(\omega_+) + \sin^2\theta e^{\frac{\omega_+}{T_R}} N_R(\omega_+)], \end{aligned} \quad (24)$$

Heat rectification in our model can be explained by possible four-wave mixing cycles which are responsible for heat flow between the left and right baths. In these cycles, the decay rates between two same dressed states of the qubits become significantly different when the thermal bias is reversed, consequently, this causes an asymmetry in the heat flow. To elaborate more on this let us look carefully at the the rates given in equation (24), we see that the rates do not only depend on the temperatures but also on the value of $\cos^2\theta, \sin^2\theta$. Now, we have already seen that for large values of ϵ these two functions differ significantly. Because of this dissimilarity, the steady state populations are not invariant under the exchange of temperature of the baths. This difference coupled with the difference in transition rates upon exchange of temperatures makes the heat flow asymmetric. Also, the rate coefficients associated with the baths exchange when we move from one heat transfer channel to the other i.e. if for a particular bath the coefficient is $\cos^2\theta$ for one channel, it becomes $\sin^2\theta$ for the

other, and since the difference in these coefficients decide rectification, this tells us that the two channels rectify in opposite directions. We will later see that this is indeed the case. For weakly interacting resonant qubits, i.e. $\omega_L = \omega_R = \omega \gg g$, an example of process which transfer heat between the baths is shown in Fig. 4. For resonant qubits, under the exchange of temperature gradient, the decay rates given in Eq. (24) become invariant, due to which asymmetry in the heat flow vanishes. To emphasize this point, we explain the zero rectification for resonant qubits using Eq. (22), heat flow becomes symmetric if

$$I_R(T_L, T_R) = -I_R(T_R, T_L), \quad (25)$$

by simple manipulation this translates to

$$D(T_L, T_R, \omega) = D(T_R, T_L, \omega), \quad (26)$$

which happens when

$$\begin{aligned} \cos^2\theta - \sin^2\theta &= 0, \\ \epsilon &= 0. \end{aligned} \quad (27)$$

Here, we note that from Eq. (16) this means that the rectification is zero for resonant qubits. This is a result we expected because we have already seen that the asymmetry of cross product is not enough and there is no other asymmetry in our model apart from the off-resonant qubits. Hence, there should be a direct relation between the rectification and that off resonance.

Looking at Fig. 5 above we see that \mathcal{R} is a non-monotonic function of both the T and g . We see that we get a plateau like stable rectifying region when one of the bath temperature is at different order of energy than the system. We also see that for strong inter-qubit coupling and less off resonance between them, the rectifying ability of the diode is pretty low. Finally we see that the direction of rectification changes sign when we exchange the qubit frequency. Now since,

$$\mathcal{R} \propto (I_R(T_R, T_L) + I_R(T_L, T_R)) \quad (28)$$

$$\begin{aligned} \mathcal{R} \propto & \frac{|\omega_D|}{\omega_D} \epsilon \left[\frac{\omega_+ (N_R(\omega_+) - N_L(\omega_+))^2}{\sqrt{1 + \epsilon^2} D(T_L, T_R, \omega_+) D(T_R, T_L, \omega_+)} \right. \\ & \left. - \frac{|\omega_-| (N_R(|\omega_-|) - N_L(|\omega_-|))^2}{D(T_R, T_L, |\omega_-|) D(T_L, T_R, |\omega_-|)} \right] \end{aligned} \quad (29)$$

Looking at the above expression we see that the two phonon energy channels compete with each other as far as rectification is concerned. For $\omega_D > 0$, the ω_+ leads to right left rectification while the ω_- channel leads to left right rectification. As a result of this, the overall rectification ability of the model is decided by which channel conducts more heat. Since the first channel is of higher energy than the second channel, for sufficiently hot baths the diode will always rectify from right to left while for low temperature baths there can be chances of the second channel contributing more. This can be seen by looking at the Fig. 5 and the above expression under appropriate approximations. Also it is clear from (29) that changing

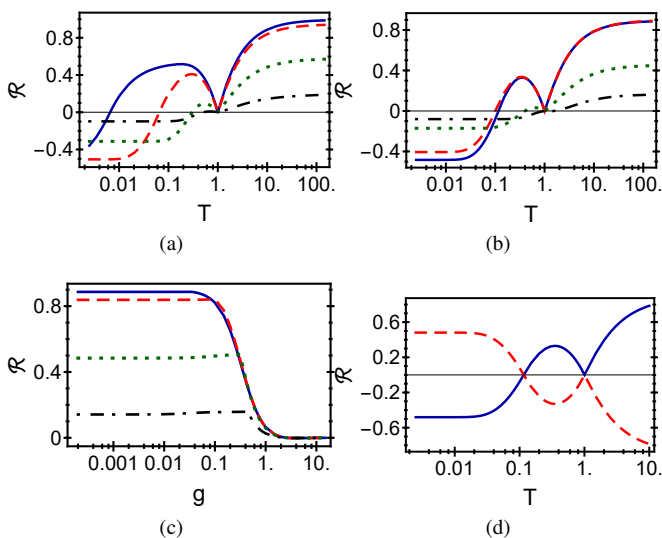


FIG. 5. (Color online) Variation of Rectification (\mathcal{R}) with T (top row) for (a) $\omega_R=0.005$ (blue solid line), $\omega_R=0.05$ (red dashed line), $\omega_R=0.4$ (green dotted line), $\omega_R=0.8$ (black dot-dashed line), for (b) $g=0.005$ (blue solid line), $g=0.05$ (red dashed line), $g=0.4$ (green dotted line), $g=0.8$ (black dot-dashed line). Variation of \mathcal{R} with ‘ g ’ (lower row) for (c) $\omega_R=0.005$ (blue solid line), $\omega_R=0.05$ (red dashed line), $\omega_R=0.4$ (green dotted line), $\omega_R=0.8$ (black dot-dashed line) with $T_R = 10$ and $T_L = 1$. Changing the sign of rectification by exchanging qubit frequencies for (d) $\omega_D > 0$ (blue solid line), $\omega_D < 0$ (red dashed line). For all the cases, the values of parameters if not otherwise specified are $\omega_R = 0.1$, $g = 0.01$, $\kappa = 0.0001$, $\omega_L = 1$, $T_{\text{ref}} = 1$.

the sign of ω_D will lead to flipping of rectification region so this is a nice control we have in our model, though the rectification values may be slightly different on such a change of sign. Finally, since the Rectification is proportional to:

$$\mathcal{R} \propto \frac{|\omega_D| \epsilon}{\sqrt{1 + \epsilon^2}} \quad (30)$$

We have an idea about the amount of off resonance we need between the qubits in our model for getting large rectification. Physically, the rectification arises due to the asymmetry in the energy levels of our system which arises due to ω_D , but if g is large in comparison to ω_D the asymmetry in energy levels is insignificant in comparison to their absolute values so the rectification decreases. This is in line with the features we see in Fig. 5.

Interestingly, from equations (19) and (29), it is clear that there is a trade off between the current and rectification in our model as the saturation current is large for small values of ϵ whereas rectification becomes very small in such a scenario and vice versa. As pointed out earlier this leads to a possibility of optimization where we can get large enough currents without compromising on the rectification ability. This feature is observed in the parametric curve given in Fig. 6(a) where we can clearly see that there is a region where the rectification remains stable while current increases before sharply falling at high current values. Ideally, this region should be targeted

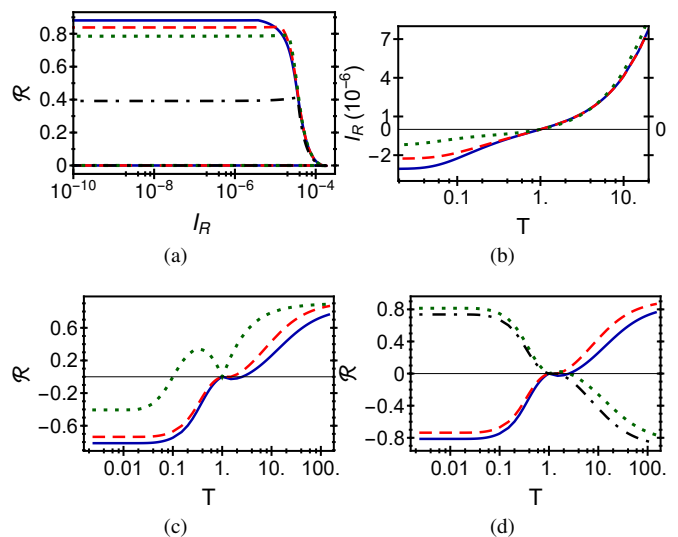


FIG. 6. (Color online)(a) Parametric curve between Rectification (\mathcal{R}) and I_R for $\omega_R=0.01$ (blue solid line), $\omega_R=0.05$ (red dashed line), $\omega_R=0.1$ (green dotted line), $\omega_R=0.5$ (black dot-dashed line) with $T_R = 10$, $T_L = 1$. Variation of I_R with T for (b) DM along x (blue solid line), along y (red dashed line), along z (green dotted line). Variation of \mathcal{R} with T for (c) DM along x (blue solid line), along y (red dashed line), along z (green dotted line). (d) Changing the sign of \mathcal{R} by exchange of qubit frequencies for DM along x (blue solid line, green dotted line) and for DM along y (red dashed line, black dot-dashed line). For all the cases the values of parameters if not otherwise specified are $\omega_R = 0.1$, $g = 0.05$, $\kappa = 0.0001$, $\omega_L = 1$, $T_{\text{ref}} = 1$.

for best performance of the diode. It is also clear from the curve that the saturation value of rectification depends on the off resonance between qubits.

C. Effect of Anisotropy Field Direction

We can see that even if we take the DM anisotropy field along different directions we get the same features in our diode as again on exchanging qubits frequencies, the rectification changes sign and we again get zero rectification for resonant qubits. However these models work better for lower temperatures as both the rectification as well as current is greater for them in those regions. This may be because there are more phonon transfer channels in these models with relatively small energies allowing the colder baths to induce transitions. However, even now for high temperatures the DM along z model works the best.

V. CONCLUSIONS

We study the rectification ability of a two qubit diode in which the qubits are interacting via the DM interaction along z directions. We see that this model works very well when the energy of off resonance of the qubits is much larger than their interaction energy. We also get high stability regions

of the diode arising when one of the temperature is of different order in energy compared to the system energy. It is also easy to change the direction of rectification in this diode by just exchanging the frequencies of the qubits. Similar features are seen when we change the direction of the anisotropy field, though such models work better for lower temperatures regions. However, for higher temperatures even now the DM along z model gives best results.

VI. ACKNOWLEDGEMENT

RM gratefully acknowledges financial support from Science and Engineering Research Board (SERB), India, under the Core Research Grant (Project No. CRG/2020/000620).

Appendix A: Master Equation

The system Hamiltonian given in section 3 can be transformed into its diagonal basis using the transformation:

$$\hat{U} = \cos^2\left(\frac{\theta}{2}\right)\hat{I}_L \otimes \hat{I}_R + \sin^2\left(\frac{\theta}{2}\right)\hat{\sigma}_L^z \otimes \hat{\sigma}_R^z + i\frac{\sin\theta}{2}(\hat{\sigma}_L^x \otimes \hat{\sigma}_R^x + \hat{\sigma}_L^y \otimes \hat{\sigma}_R^y) \quad (\text{A1})$$

The relation between the operators in new (dressed) basis with the operators in old (computational) basis is:

$$\tilde{A} = \hat{U}^\dagger \hat{A} \hat{U} \quad (\text{A2})$$

$$\hat{A} = \tilde{U} \tilde{A} \tilde{U}^\dagger \quad (\text{A3})$$

where \tilde{A} is the operator in dressed basis and \hat{A} is the operator in computational basis. It can be proved that under the transformation \hat{U} , the system Hamiltonian becomes a diagonal matrix with the following form in terms of dressed operators:

$$\tilde{H}_S = \frac{(\omega_S + \Omega)}{2} \tilde{\sigma}_L^z + \frac{(\omega_S - \Omega)}{2} \tilde{\sigma}_R^z \quad (\text{A4})$$

Now we want to write the system interaction operators in terms of these dressed operators. Using equation (A2), we have:

$$\hat{\sigma}_i^x = \tilde{U} \tilde{\sigma}_i^x \tilde{U}^\dagger \quad (\text{A5})$$

with i either left or right and:

$$\tilde{U} = \cos^2\left(\frac{\theta}{2}\right)\tilde{I}_L \otimes \tilde{I}_R + \sin^2\left(\frac{\theta}{2}\right)\tilde{\sigma}_L^z \otimes \tilde{\sigma}_R^z + i\frac{\sin\theta}{2}(\tilde{\sigma}_L^x \otimes \tilde{\sigma}_R^x + \tilde{\sigma}_L^y \otimes \tilde{\sigma}_R^y) \quad (\text{A6})$$

Performing the above calculations, we get:

$$\begin{aligned} \hat{\sigma}_L^x &= \cos\theta \tilde{\sigma}_L^x + \sin\theta \tilde{\sigma}_L^z \tilde{\sigma}_R^y \\ \hat{\sigma}_R^x &= \cos\theta \tilde{\sigma}_R^x + \sin\theta \tilde{\sigma}_L^y \tilde{\sigma}_R^z \end{aligned} \quad (\text{A7})$$

The interaction picture version of these operators is ($e^{i\tilde{H}_S t} \tilde{A} e^{-i\tilde{H}_S t}$):

$$\hat{\sigma}_L^x(t) = e^{-i(\omega_S + \Omega)t} \cos\theta \tilde{\sigma}_L^- + i e^{-i(\omega_S - \Omega)t} \sin\theta \tilde{\sigma}_L^z \tilde{\sigma}_R^- + H.C. \quad (\text{A8})$$

$$\hat{\sigma}_R^x(t) = e^{-i(\omega_S - \Omega)t} \cos\theta \tilde{\sigma}_R^- + i e^{-i(\omega_S + \Omega)t} \sin\theta \tilde{\sigma}_L^- \tilde{\sigma}_R^z + H.C. \quad (\text{A9})$$

Once we know the interaction picture operators it is easy to infer the master equation given in (12).

Appendix B: Heat Current

Again from the master equation (12), we can see that:

$$\begin{aligned} \mathcal{L}_R \hat{\rho}(t) &= \kappa [\cos^2\theta (G_R(\omega_-) \mathcal{D}(\tilde{\sigma}_R^-) + G_R(-\omega_-) \mathcal{D}(\tilde{\sigma}_R^+)) \\ &\quad + \sin^2\theta (G_R(\omega_+) \mathcal{D}(\tilde{\sigma}_L^- \tilde{\sigma}_R^z) + G_R(-\omega_+) \mathcal{D}(\tilde{\sigma}_L^+ \tilde{\sigma}_R^z))] \end{aligned} \quad (\text{B1})$$

Using definition of current (18), we get:

$$\begin{aligned} I_R &= \kappa \left[\frac{\omega_+}{2} [\sin^2\theta (-G_R(\omega_+) \langle I + \tilde{\sigma}_L^z \rangle + G_R(-\omega_+) \langle I - \tilde{\sigma}_L^z \rangle)] \right. \\ &\quad \left. + \frac{\omega_-}{2} [\cos^2\theta (-G_R(\omega_-) \langle I + \tilde{\sigma}_R^z \rangle + G_R(-\omega_-) \langle I - \tilde{\sigma}_R^z \rangle)] \right] \end{aligned} \quad (\text{B2})$$

We can find the dynamic equations of the average quantities required above:

$$\begin{aligned} \frac{d\tilde{\sigma}_L^z}{dt} &= \kappa [\cos^2\theta (-G_L(\omega_+) \langle I + \tilde{\sigma}_L^z \rangle + G_L(-\omega_+) \langle I - \tilde{\sigma}_L^z \rangle) \\ &\quad + \sin^2\theta (-G_R(\omega_+) \langle I + \tilde{\sigma}_L^z \rangle + G_R(-\omega_+) \langle I - \tilde{\sigma}_L^z \rangle)] \end{aligned} \quad (\text{B3})$$

$$\begin{aligned} \frac{d\tilde{\sigma}_R^z}{dt} &= \kappa [\sin^2\theta (-G_L(\omega_-) \langle I + \tilde{\sigma}_R^z \rangle + G_L(-\omega_-) \langle I - \tilde{\sigma}_R^z \rangle) \\ &\quad + \cos^2\theta (-G_R(\omega_-) \langle I + \tilde{\sigma}_R^z \rangle + G_R(-\omega_-) \langle I - \tilde{\sigma}_R^z \rangle)] \end{aligned} \quad (\text{B4})$$

For finding the steady state solution the L.H.S. of both the equations above goes to zero. Using the steady state value of the above averages and putting it in the expression of current (B2) gives us the analytical form of the current in (19).

-
- [1] V. Balachandran, G. Benenti, E. Pereira, G. Casati, and D. Poletti, *Phys. Rev. E* **99**, 032136 (2019).
- [2] G. T. Landi, E. Novais, M. J. de Oliveira, and D. Karevski, *Phys. Rev. E* **90**, 042142 (2014).
- [3] J. Ordonez-Miranda, Y. Ezzahri, and K. Joulain, *Phys. Rev. E* **95**, 022128 (2017).
- [4] D. Segal and A. Nitzan, *Phys. Rev. Lett.* **94**, 034301 (2005).
- [5] C. Kargı, M. T. Naseem, T. c. v. Opatrný, O. E. Müstecaplıođlu, and G. Kurizki, *Phys. Rev. E* **99**, 042121 (2019).
- [6] M. Terraneo, M. Peyrard, and G. Casati, *Phys. Rev. Lett.* **88**, 094302 (2002).
- [7] B. Li, L. Wang, and G. Casati, *Phys. Rev. Lett.* **93**, 184301 (2004).
- [8] J. Lan and B. Li, *Phys. Rev. B* **74**, 214305 (2006).
- [9] M. R. Kaushik Saurabh, Kaushik Sachin, *Eur. Phys. J. B* (2018).
- [10] S. Lepri, R. Livi, and A. Politi, *Phys. Rep.* **377**, 1 (2003).
- [11] O.-P. Saira, M. Meschke, F. Giazotto, A. M. Savin, M. Möttönen, and J. P. Pekola, *Phys. Rev. Lett.* **99**, 027203 (2007).
- [12] W. Chung Lo, L. Wang, and B. Li, *J. Phys. Soc. Jpn.* **77**, 054402 (2008).
- [13] M. T. Naseem, A. Misra, O. E. Müstecaplıođlu, and G. Kurizki, *Phys. Rev. Research* **2**, 033285 (2020).
- [14] J. W. Jiang, J. S. Wang, and B. Li, *Europhys. Lett.* **89**, 46005 (2010).
- [15] J. P. S. Peterson, T. B. Batalhão, M. Herrera, A. M. Souza, R. S. Sarthour, I. S. Oliveira, and R. M. Serra, *Phys. Rev. Lett.* **123**, 240601 (2019).
- [16] J. Hwang, M. Pototschnig, R. Lettow, G. Zumofen, A. Renn, S. Götzinger, and V. Sandoghdar, *Nature* **460** (2009).
- [17] Y. Shen, M. Bradford, and J.-T. Shen, *Phys. Rev. Lett.* **107**, 173902 (2011).
- [18] K. Micadei, J. P. S. Peterson, A. M. Souza, R. S. Sarthour, I. S. Oliveira, G. T. Landi, T. B. Batalhão, R. M. Serra, and E. Lutz, *Nat. Commun.* **10**, 2456 (2019).
- [19] N. Yang, G. Zhang, and B. Li, *Appl. Phys. Lett.* **95**, 033107 (2009).
- [20] N. Li, J. Ren, L. Wang, G. Zhang, P. Hänggi, and B. Li, *Rev. Mod. Phys.* **84**, 1045 (2012).
- [21] A. Dhar, *Adv. Phys.* **57**, 457 (2008).
- [22] I. Dzyaloshinsky, *J. Phys. Chem. Solids* **4**, 241 (1958).
- [23] T. Moriya, *Phys. Rev.* **120**, 91 (1960).
- [24] H. P. Breuer and F. Petruccione, *The theory of open quantum systems* (Oxford university press, 2002).
- [25] A. Levy and R. Kosloff, *Europhys. Lett.* **107**, 20004 (2014).
- [26] M. T. Naseem, A. Xuereb, and O. E. Müstecaplıođlu, *Phys. Rev. A* **98**, 052123 (2018).
- [27] T. Werlang, M. A. Marchiori, M. F. Cornelio, and D. Valente, *Phys. Rev. E* **89**, 062109 (2014).
- [28] R. Kosloff, *Entropy* **15**, 2100 (2013).
- [29] A. Levy and R. Kosloff, *Europhys. Lett.* **107**, 20004 (2014).